

An Integrated Radar-Infrasound Network for Meteorological Infrasound Detection and Analysis

David Pepyne, Michael Zink, Jerald Brotzge, Eric Knapp, Alexander Mendes, Brian McCarthy, Sean Klaiber, and Bettina Benito-Figueroa

21 February 2011

Abstract

The atmosphere generates numerous signals that can be used for weather hazard detection and early-warning. For short-term detection and tracking of rapidly evolving weather, such as tornadoes, ground-based weather radar is the primary sensor used today. But these radars have a number of fundamental limitations in terms of temporal sampling rate and low-altitude blockage that can hinder their effectiveness. Because of its potential to overcome the coverage limitations of radar, infrasound has been proposed as a complementary technology to be used alongside radar in a tornado early-warning system. Previous work by NOAA has shown that infrasound can be used to detect tornadoes and their precursors, but was not able to demonstrate any actual operational improvements in tornado early-warning. Theory suggests that these previous efforts failed to show infrasound's operational early-warning capabilities primarily because the infrasound sites were spaced too far apart. This paper describes an experiment to be conducted in the spring of 2011 by the NSF Engineering Research Center for Collaborative Adaptive Sensing of the Atmosphere (CASA) to revisit the infrasound-radar early-warning concept but with a much closer spacing of both the infrasound sites and the radar sites (30 km between sites vs. the ~250 km between sites using in previous studies). This close spacing should maximize the probability of detection and location of infrasound sources within 2 minutes of their initial emission.

1. Introduction

An important problem to the U.S. National Weather Service (NWS) is increasing tornado lead time (Berchhoff, 2010; Kelleher & Melendez, 2010). Currently the average tornado lead-time is 13-14 minutes nationwide, but every increase in lead-time improves public safety, a 30 minute to 1 hour lead time (warn on forecast) is an NWS goal (Berchhoff, 2010; Kelleher & Melendez, 2010; see also: <http://www.vortex2.org/home/>). Today ground-based radar

AFFILIATIONS: Pepyne, Zink, Knapp, and Klaiber – University of Massachusetts, Amherst, Massachusetts; Brotzge – University of Oklahoma, Norman, Oklahoma; Mendes – Vanderbilt University, Nashville, Tennessee; McCarthy – Western New England College, Springfield, Massachusetts; Benito-Figueroa – University of Puerto Rico, Mayaguez, Puerto Rico.

CORRESPONDING AUTHOR: David Pepyne, University of Massachusetts, 151 Holdsworth Way, Amherst, MA 01003. E-mail: pepyne@ecs.umass.edu.

(GBR) is the primary instrument used by NWS forecasters to make tornado warning decisions. For radar, line-of-sight (LOS) is needed between the radar and the tornado target. This results in coverage limitations, both temporally due to the volume scan time and at low-altitude due to terrain blockage and earth curvature. In particular, the large spacing between today's WSR-88D weather surveillance radars prevents coverage of the lowest portions of the atmosphere where tornado funnels and their debris signatures occur (NRC 1995, 2002, 2004, 2009). These low-altitude coverage limitations (see Fig. 1) can hinder tornado early-warning.

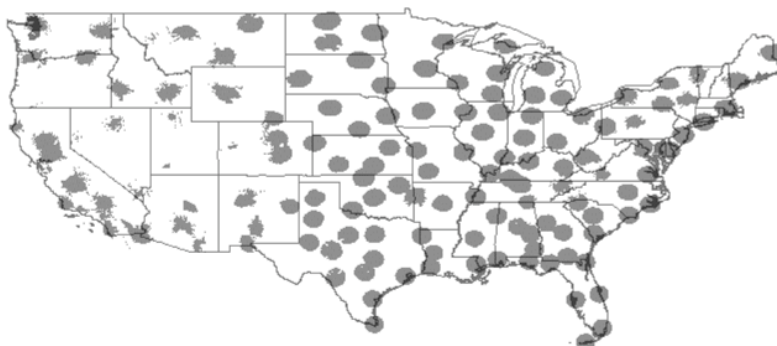


Fig. 1. WSR-88D coverage at 1000 feet above-ground-level (AGL) (from (McLaughlin et al, 2009)).

In addition to the commonly described audible “freight-train” sounds, work by Bedard et al at NOAA’s Earth System Research Laboratory (ERSL) has demonstrated that tornadoes and their precursors also produce sub-audible, very low-frequency (< 20 Hz) infrasound (Bedard and Georges, 2000; Bedard et al, 2004a, 2004b, Bedard, 2005; Schecter et al 2008). This motivated the consideration of using infrasound for tornado early warning. With respect to this, infrasound is particularly useful in that (i) it does not require line-of-sight (LOS) between the infrasound emitter and the infrasound sensing instrument, (ii) it experiences very little amplitude attenuation with distance traveled, and (iii) it is omnidirectional, propagating out simultaneously in all directions from the infrasound emitter (tornado) at once.

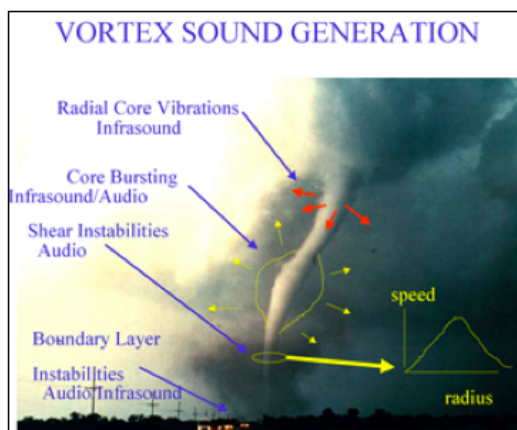


Fig. 2. Audible and sub-audible sources of sound generated by tornadoes (from the NOAA ISNet website: <http://www.esrl.noaa.gov/psd/programs/infrasound/isnet/>).

In a project called ISNet (short for infrasound network), Bedard et al (2004a) deployed three infrasound monitoring stations roughly collocated with the WSR-88D radars at Boulder, CO, Goodland, KS, and Pueblo, CO respectively. This siting, shown in Fig. 3, put the ISNet stations approximately 250km apart.

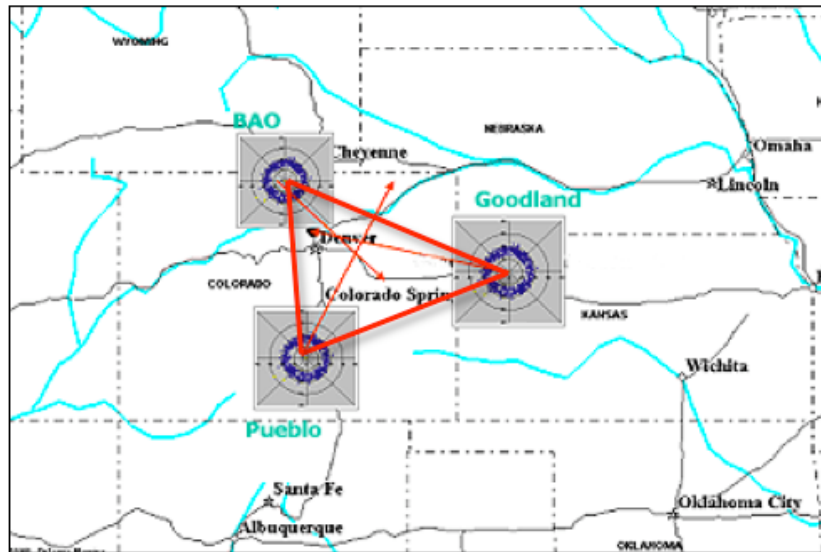


Fig. 3. Locations of the three stations in the ISNet infrasound monitoring network (from the NOAA ISNet website: <http://www.esrl.noaa.gov/psd/programs/infrasound/isnet/>).

The concept of the ISNet was to use infrasound to overcome the temporal and low-altitude coverage limitations of the WSR-88D radars by providing acoustic coverage while the radar was looking up high or in some other direction, and by providing coverage behind terrain or at low-altitude where the radar does not have LOS. Results over two tornado seasons were very promising with post-event analysis showing numerous cases where infrasound emissions from confirmed tornado events were detected at ISNet stations. Moreover, the results showed that in many cases, infrasound detections actually began several 10's of minutes to more than an hour prior to the confirmed time of tornado touchdown (Bedard et al, 2004b). The difficulties were in distinguishing tornado precursors from non-tornadic infrasound signals (false-alarms), and in determining the location of the infrasound source in real-time so that the detections might be useful for operational decision making.

The contributions of this paper are two-fold. First, we present an infrasound propagation analysis that concludes that for operational improvements in lead-time, an infrasound network with a much closer spacing between the infrasound stations than the 250km used in the ISNet study is needed. The second contribution is a description of the hardware and software being developed for an experiment that the NSF Engineering Research Center (ERC) for Collaborative Adaptive Sensing of the Atmosphere (CASA) (McLaughlin et al, 2009) will be conducting starting this spring (2011) to integrate infrasound into its Oklahoma radar test bed located just to the southwest of Oklahoma City (Brewster et al, 2005). The CASA radar test bed, which CASA has been operating since 2006, is comprised of four small, short-wavelength (X-band), boundary-layer observing radars spaced 30km

apart (see Fig. 4). By collocating infrasound stations with the CASA radars a spacing between infrasound stations is achieved that an infrasound propagation analysis shows should maximize the ability to both detect and locate infrasound emitters less 2 minutes after they begin their infrasound emissions. The use of the CASA test bed will allow for the real-time correlation of any infrasound detections with the rest of the CASA weather hazard warning infrastructure (CASA radar data, NEXRAD radar data, tornado spotter reports, nowcasts, forecasts, NWP models, forecaster analysis, and so on (cf. Brotzge et al, 2007, 2010; Philips et al, 2010) allowing for an understanding of infrasound signatures, detection rates, false alarm rates, and methods for presentation to operational forecasters.

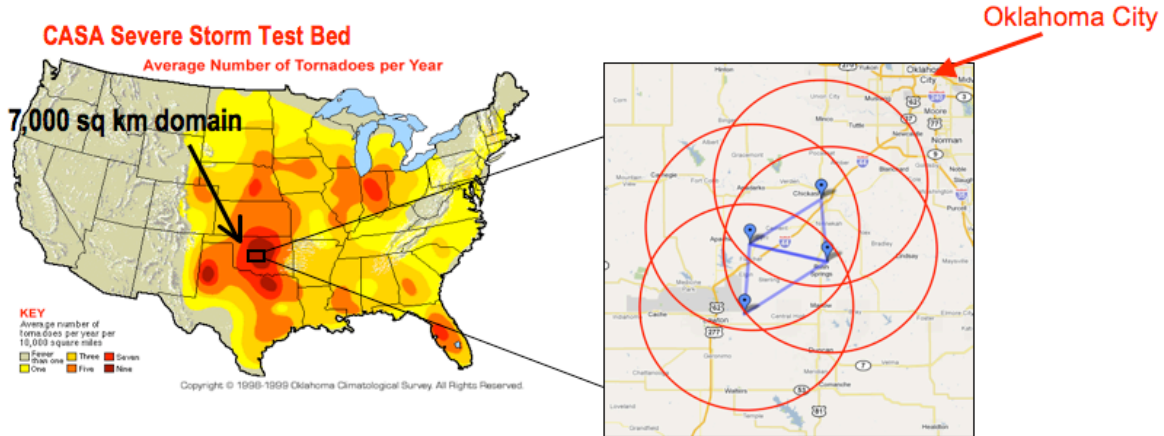


Fig. 4. Four node, boundary-layer observing CASA radar test bed network in the heart of “tornado alley” in Oklahoma. The radars are approximately arranged as two back-to-back equilateral triangles with 30 km spacing between radars (Brewster et al, 2005). The radars have 40 km range to exploit multiple simultaneous views from different ranges and aspect angles (McLaughlin et al, 2009). Tornado density map courtesy the Oklahoma Climatological Survey.

The remainder of this paper is organized as follows. Section 2 presents an infrasound propagation analysis to determine the infrasound station spacing suitable for real-time decision making from infrasound detections. Section 3 describes CASA’s planned infrasound experiment to understand infrasound and how it might be used for operational forecasting and warning. Section 4 describes in some detail the design of the infrasound stations to be deployed, including descriptions of the sensors, spatial wind filters, and data loggers. Section 5 describes the software and visual displays developed for the experiment. The paper closes in Section 6 with a summary and conclusions.

2. Infrasound Propagation Analysis

The goal of this project is to design and deploy an infrasound system that improves weather-hazard (e.g., tornado) early-warning. Let us take this to mean that the system must detect the infrasound signal from a weather hazard (or its precursors) no more than 2 minutes after the initial emission of the signal (which is about half the time between WSR-88D volume scans). The speed of sound is a function of temperature and local wind speed. Nominally the speed of sound in the (standard, 20 deg C) atmosphere is 343m/s (1,236

km/hr). At 343 m/s the propagation time is non-negligible (unlike radar, where propagation delays are determined by the $3e8$ m/s speed of light): 20 km \approx 1 minute, 40 km \approx 2 minutes, 100 km \approx 5 minutes, 200 km \approx 10 minutes, and so on. For a 2-minute detection delay, we therefore need an infrasound station no more than 40 km from the infrasound source. This will give detection, but it will not give range. Unlike a WSR-88D radar, which gives azimuth, range, and radial velocity, an infrasound station can only give the azimuth to the infrasound source, i.e., an infrasound station can only determine the direction from which the sound is arriving. Thus, with detection at only a single infrasound station, range is ambiguous, and due to the very low attenuation of the amplitude of infrasound signals with range, can be from very close or from many hundreds of kilometers distant. The ISNet setup, for example, recorded tornado detections from more than 500km from the infrasound stations (Bedard et al, 2004b).

To get range with infrasound, detection at multiple stations is needed. For example, suppose we have detections at two stations numbered 1 and 2 respectively. Let the azimuth of arrival of the signal at station 1 be θ_1 and at station 2 be θ_2 . Then if LAT_1, LON_1 is the (latitude, longitude) location of station 1 and LAT_2, LON_2 is the location of station 2, we can use the formula for intersecting radials from (Williams, 2010) to infer the LAT, LON location of the infrasound detection. This would suggest the need for 2 or more infrasound stations within 40 km of a weather hazard. A repeating network triangular unit cells with 40 km between infrasound stations, like that shown in Fig. 5 would satisfy this condition.

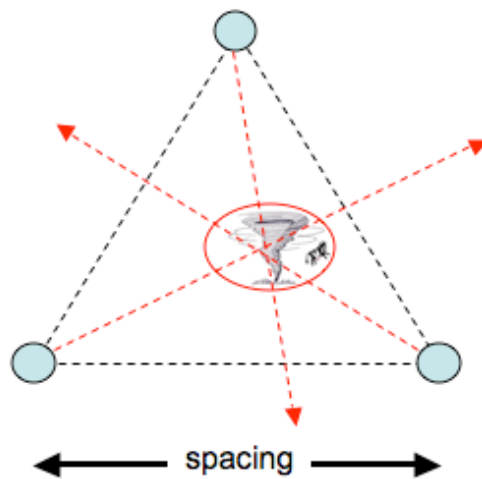


Fig. 5. Unit cell of an infrasound network. The network is made up of repeating patterns of these triangular unit cells. A spacing of 40 km between infrasound stations would allow the network to locate an infrasound source within 2-minutes after initial infrasound emission.

On the other hand, although a 40 km spacing between infrasound stations would put infrasound emitters no more than 40 km from a target, it may not be close enough to ensure with high probability that detection would be detected at multiple nearest-neighbor stations (i.e., stations within 40 km of one another). The reason has to do with the way infrasound propagates in the atmosphere. Because the speed of sound is dominated by

temperature and because temperature initially tends to decrease with increasing altitude (on a standard day), sound is initially refracted upwards as it moves away from its source. This upward refraction continues until the sound reaches ~40 km altitude at which point heating in the ozone layer reverses the refraction, bending the sound waves back down to the ground. The result is that the atmosphere acts like a huge waveguide to create, for an acoustic sensor on the ground, three propagation zones. These zones, illustrated in Fig. 6, are a *direct zone* where sound follows the earth's curvature (this zone extends from 0-20/30km); an *acoustic shadow zone* where the sound has been ducted up and away from the earth's surface so that a sensor on the ground may not hear the infrasound source (this zone extends to ~200km); and a *bounce zone* where the sound returns to the surface and can again be heard by infrasound sensors on the ground (Drob et al., 2003). Note that the direct propagation zone is our interest here, since the bounce zone being ≥ 200 km from the source represents sounds that are ≥ 10 minutes old, and hence generally not useful for early-warning decision making. In addition, it is also important to note that the range of the direct propagation zone is heavily dependent on the temperature lapse rate with altitude and with local surface winds – it is extended downwind and can disappear entirely at night and during temperature inversions (cf. Bedard and Georges, 2000).

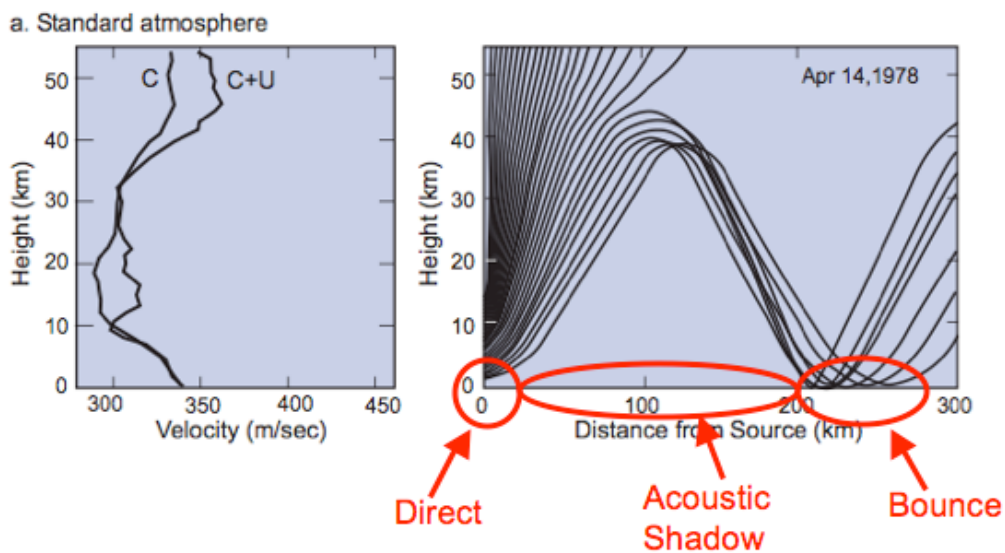


Fig. 6. Acoustic waveguide created by the decrease of temperature with altitude showing the direct, acoustic shadow (aka skip), and bounce zones. Infrasound sensors located on the ground in the acoustic shadow region will not hear the infrasound signal; infrasound sensors in the bounce zone are hearing infrasound signals that are more than 10 minutes delayed, and hence not generally useful for early-warning decision making. Figure from (Skowbo et al, 2009).

The conclusion to be drawn is that for an infrasound early-warning system the infrasound stations should be placed in a network with spacing between stations of no more than 20-30 km. This maximizes the probability that two or more infrasound stations will be in the direct propagation path of the infrasound signal, which will meet our early-warning

requirements of detection no more than 2 minutes after initial emission (for early-warning decision making) by two or more sites (for source location).

3. CASA Infrasond Experiment

From the previous section, the concept-of-operations (CONOPS) of an infrasond early-warning system would be as follows: An infrasond signal is detected at two or more stations; from the back-azimuth vectors computed at the stations, the location of the infrasond source is geo-located and compared with radar and other sources of weather information about that location; the process is repeated over a moving window of infrasond data in order to track the motion of the infrasond emitter.

To assess the value of infrasond for weather hazard diagnosis and early-warning, CASA will revisit the NOAA ISNet experiment, but on a spacing between infrasond stations of 30 km. This spacing will be achieved by collocating infrasond stations with the Cyril (KCYR) and Rush Springs (KRSP) radars in the CASA Oklahoma radar test bed. The test bed location and proposed infrasond station locations are shown in Fig. 7. While 40 km is the maximum for 2-minute detection delay, 30 km increases the probability of avoiding acoustic shadowing.

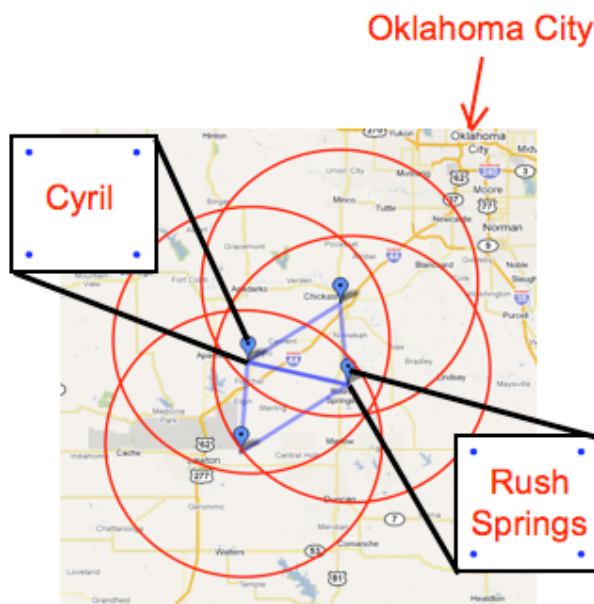


Fig. 7. CASA radar test bed in Oklahoma showing where the two infrasond stations to be deployed for the Spring 2011 CASA infrasond experiment will be located.

The infrasond detections will be integrated into CASA's end-to-end weather hazard prediction, forecasting, warning and response system operated out of the NSSL Hazardous Weather Test Bed in the NWS building on the southern part of the Oklahoma University campus. The infrasond detections will be displayed to researchers and forecasters along with other weather products, including CASA's radar data, NEXRAD radar data, NWP predictions, multi-Doppler wind estimates, 3DVAR winds, spotter reports, and so on

(Brotzge et al 2007; Philips et al, 2007). Infrasound detections that geo-locate inside the domain of the CASA radar test bed will be analyzed and acted upon in real-time using CASA radar data; detections geo-locating outside the test bed will be analyzed post-experiment. The analysis will seek to understand the types of infrasound detections, signatures, etc. that occur during severe weather and to appraise the value of infrasound for severe weather diagnosis and early-warning (through measures such as POD, FAR, and potential lead time improvements).

A blowup of an individual infrasound station is shown below in Fig. 8. The figure shows each station as consisting of four infrasound sensors arranged into an 80 by 80 meter array. This array of four sensors forms the “antenna aperture” for the back-azimuth angle-of-arrival estimation process (to be described in Section 5). Each sensor has attached to it a 15.24 meter (50 foot) diameter spatial wind filter to reduce the noise due to wind turbulence. Each sensor is wired to a central data logger where the infrasound pressure samples are collected and served (over socket connections) to the signal processing algorithms for back-azimuth and infrasound source geo-location. The logger is bolted to the radar tower so that it can tap into the radar’s electric power system and reach the public Internet over the radar’s communication links. Each infrasound station also has a weather station collocated with one of the infrasound sensors for recording the wind speed, direction, ambient temperature, humidity, and rainfall at the site. As with the CASA radars, all monitoring, operation, and data access is via secure socket connections over the public Internet.

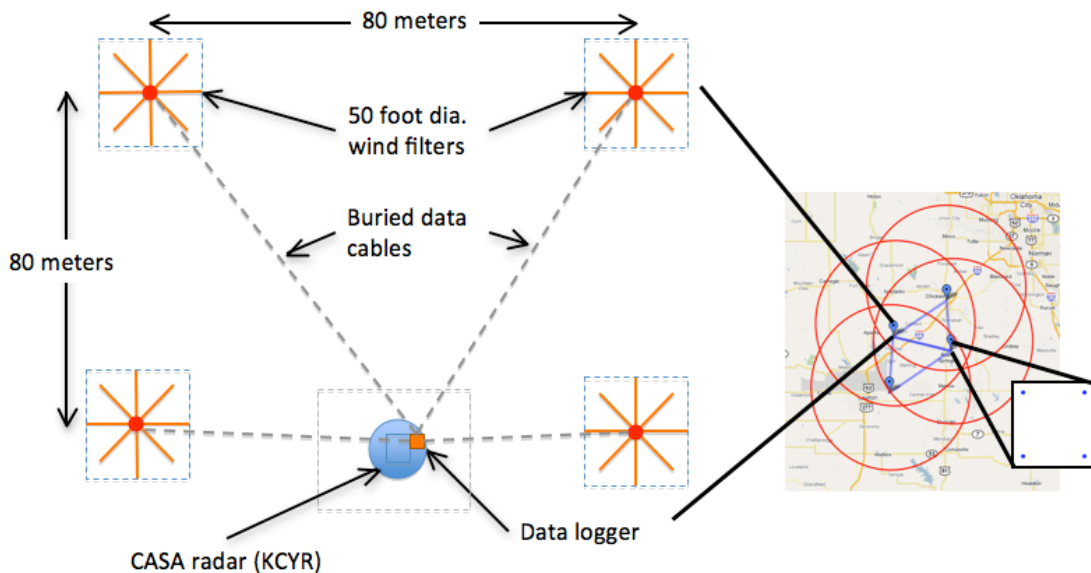


Fig. 8. Blowup of an infrasound site for the CASA infrasound experiment.

4. Hardware Details

This section details the infrasound site components in Fig. 8.

4.1 Infrasound Sensors

The sensors used are Model 6000-16B barometers manufactured by Paroscientific, Inc. of Redmond WA (<http://www.paroscientific.com/>). These barometers work by converting the vibration frequency of a quartz crystal resonator into highly accurate measurements of barometric pressure (NIST traceable to 0.01% accuracy). Approximately the size of a human fist, these barometers were chosen because they are easy to operate and satisfy all the requirements for the infrasound application. First, they have identical response characteristics, which is necessary for the determination of back-azimuth, angle of arrival estimation (to be described in Section 5), and results from the Model 6000-16B being fully calibrated, temperature compensated barometers. Moreover, this calibration is very stable, eliminating the need for the expensive calibrations required of the differential microbarographs typically used for infrasound applications (such as nuclear test ban treaty compliance, cf, Christie and Campus, 2010). Second, they have built-in, software configurable anti-alias filters (5-pole rolloff) necessary to eliminate high-frequency energy folding into the infrasound band. Third, the barometers respond to extremely small changes in pressure, with better than 0.01Pa (10e-7 bar) resolution at 40 Hz sample rate. The barometers are inherently digital, outputting their data in human readable ASCII over an RS232/RS485 interface (RS485 for large size arrays requiring long cable lengths), eliminating the need for A/D converters. The barometers have a proven track record for infrasound detection capability, including volcano eruptions, boldes, sonic booms, and so on (Schaad, 2009). Fig. 9 shows the barometer and its resolution as a function of sample period, Fig. 10 shows an example of microbaroms detection recorded on 29 December 2010 at the end of the North-Easter that blew up the U.S. east coast just after Christmas 2010. These data were recorded in northern Vermont using a laptop setup inside a house. Microbaroms are caused by storms at sea (cf, Olson and Szuberla, 2005). They are lower in frequency than tornadoes (microbaroms occur in the 0.1-0.3 Hz range; tornadoes are typically ~1 Hz), but make a good test signal since synthetic infrasound test signals are very difficult to generate while microbaroms can be regularly detected almost everywhere.

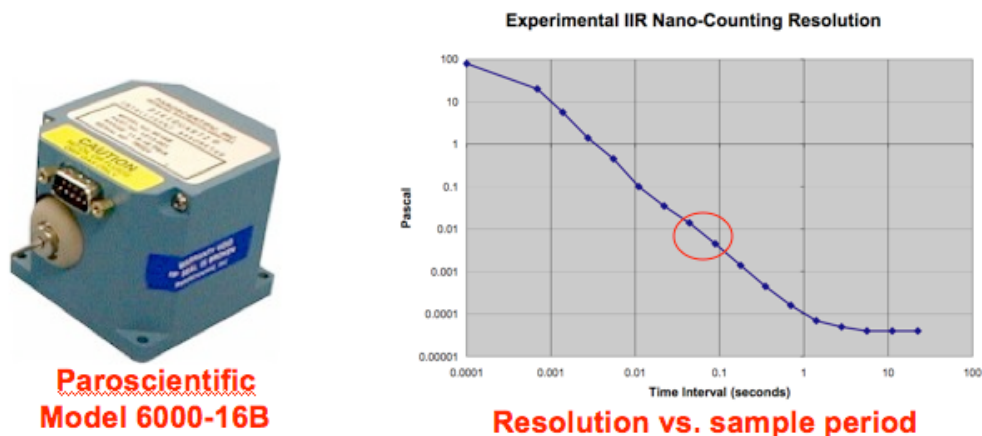


Fig. 9. Paroscientific Model 6000-16B, showing its resolution as a function of sample period.

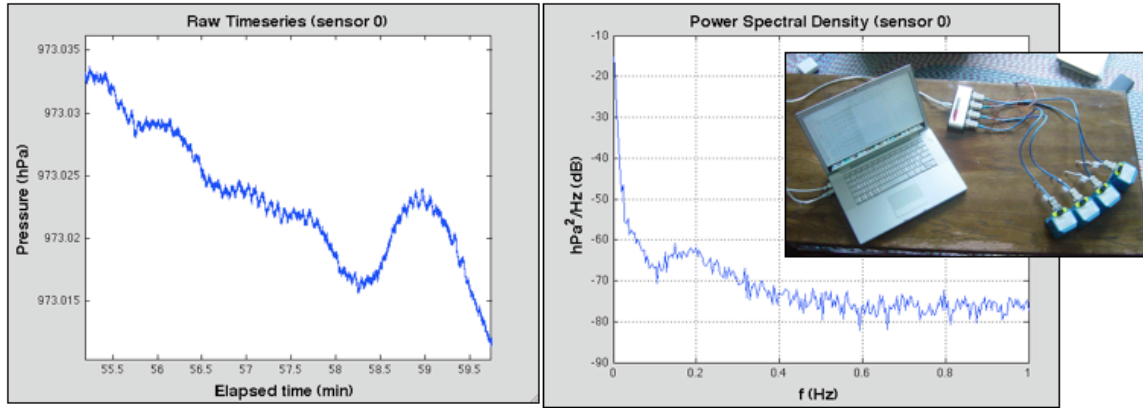


Fig. 10. Weak microbaroms recorded with the Paroscientific Model 6000-16B during a North Easter that traveled up the U.S. east coast over Christmas 2010. For these results, the barometers were connected to a laptop inside a house in northern Vermont.

4.2 Spatial Wind Filter

Because the infrasound sensors at a site are positioned on the ground, they are subject to turbulence when the wind is blowing. The typical way to reduce wind turbulence is with a spatial wind filter attached to each infrasound sensor. A spatial wind filter is composed of pipes or micro-porous (“soaker”) hoses with many holes distributed over a spatial area extending radially around the infrasound sensor. The principle of operation of a spatial wind filter is that, because turbulence is spatially coherent over small spatial scales (meters) while infrasound signals are coherent over large spatial scales (100’s of meters), summing the pressure contributions from a large number of holes spatially distributed over a large physical area increases the signal-to-noise-ratio (SNR) by constructively summing the infrasound signal while destructively summing the turbulence (Walker and Hedlin, 2010). Similar to the ISNet project, the CASA infrasound experiment will use a 50 foot diameter radial arrangement of micro-porous hoses each attached at a summing junction which itself is connected (through a moisture collector) to the Paroscientific barometer. The barometer is protected inside a weather sealed 5-gallon paint bucket. Fig. 11 shows the spatial wind filters developed for the CASA infrasound project. The spectrograms in Fig. 12 show some turbulence filtering results.

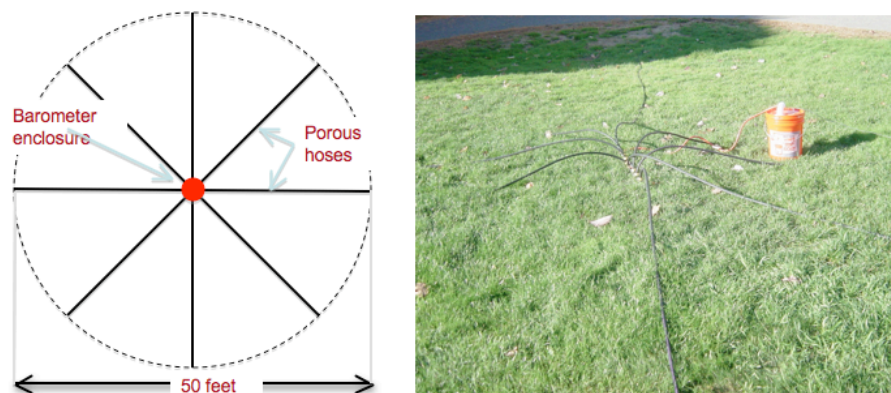


Fig. 11. Spatial wind filter developed for the CASA infrasound experiment.

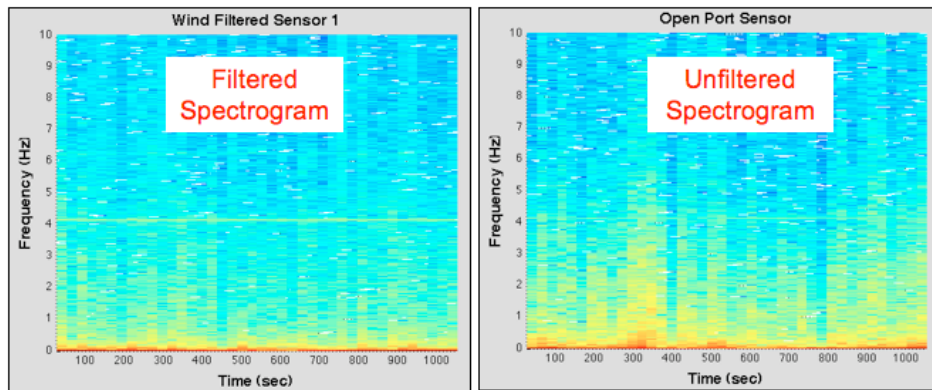


Fig. 12. Pressure spectrograms with (lef) and without (right) wind filtering showing the reduction in wind induced turbulence noise.

4.3 Data Loggers

Power and communications to the barometers is supplied through RS485 cables running from the barometers to a data logger computer attached to the radar tower. The data loggers were constructed in-house by undergraduate students (funded through the NSF Research Experience for Undergraduates (REU) program). The data loggers are designed for “on-the-grid” or “off-the-grid” deployments. On-the-grid deployments, which is how they will be used in the experiment being described in this paper, take power from an a/c power cord and send communications through an Ethernet cable plugged into an Internet switch. Off-the-grid deployments take power from battery or solar charged battery and use a wireless radio link or reverse SSH through a GSM/GPRS modem to connect to the Internet. A schematic showing the major parts of the data logger is shown in Fig. 13.

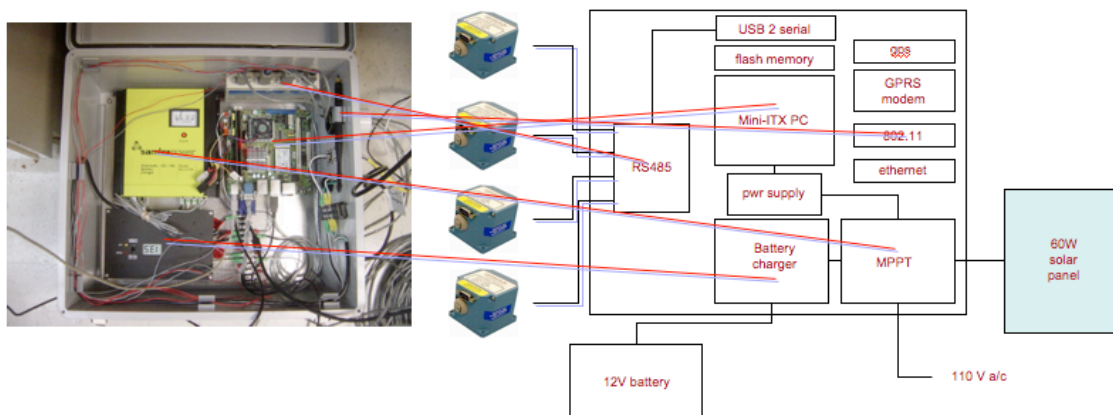


Fig. 13. Data logger showing major component parts.

5. Software Details

Software running in each data logger, which use the Ubuntu UNIX OS (<http://www.ubuntu.com/>), configures the barometers, paces the barometer sample rate,

runs monitoring and control programs, sends the barometer measurements over TCP socket connections to a data archive (the data archive will be at the University of Massachusetts, Amherst, MA), and sends the barometer measurements, again via TCP socket connections to programs for infrasound analysis, back-azimuth estimation, and web display. Fig. 14 shows the major software components and their organization. As shown in the figure, the software is organized as a collection of client/server programs. The main data-acquisition/data-server program is *dqtsserver*. This program is written in C and is responsible for populating the basic data structures <siteinfo>, <configinfo>, and <sample>. As its name implies, <siteinfo> contains information about the infrasound site – its name, location, number of barometers, barometer type, model, firmware version, serial numbers, barometer positions in the array, and so on. The data structure <configinfo> contains information about the barometer configuration settings such as the pressure units, temperature units, nano-resolution mode settings, anti-alias filter cutoff frequency, sample rate, and so on. The data structure <sample> contains a sample counter along with the time-stamped pressure measurements themselves.

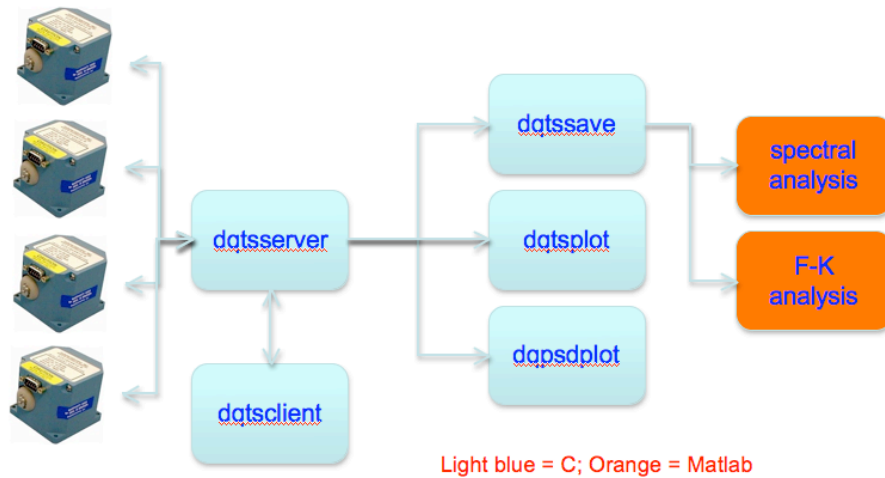


Fig. 14. Data logger software components and organization.

The <siteinfo>, <configinfo>, and <sample> data structures are served via TCP sockets as XML messages to a number of client programs. Client programs ingesting these messages include *dqtssave*, a client program to save the XML messages directly as received into an ASCII XML file; *dqtspot* a client program to plot the time-series sample data to the console for monitoring infrasound station operation and status; and *dqpsdplot* for plotting periodograms, again as a check of station operation and status. Fig. 15 below shows example plots from *dqtspot* and *dqpsdplot*.

The final client program is *dqtscclient*. This client program controls the *dqtsserver* and *dqtssave* programs, which run as daemons, allowing a local or remote operator to change configuration settings such as the sample rate and anti-alias cutoff frequency on-the-fly, and to toggle data saving on and off as desired.

Note that only *dqtsserver* needs to run locally on the data logger computer. The client programs can run locally or remotely over the public Internet. We do remark though that it

is generally safer to run *dqtssave* locally on the data logger to avoid TCP buffer overflow and resultant data loss should the TCP/IP connection be slow or get interrupted.

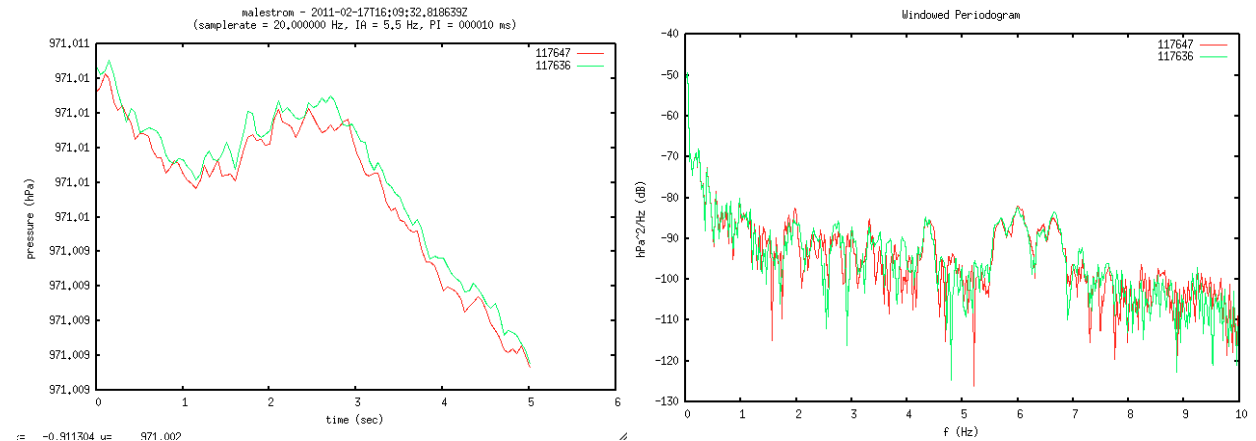


Fig. 15. Example time-series plot from *dqtplot* (left) and periodogram plot from *dqpsdplot* (right).

5.1 Sample Rate Control and Time-Stamping

Before moving on to describe the Matlab analysis programs in Fig. 14, let us first explain how *dqtserver* achieves “synchronized” sampling and proper time-stamping of the data from the array of four barometers. The basic idea is that the barometers are configured to “immediately” return a measurement in response to a “trigger” command. The sampling loop in *dqtserver* then operates as shown in Table 1 below.

Table 1. *dqtserver* sampling loop.

1. Wait for a 0.05 second timeout to expire (for a 20Hz sample rate). In particular, wait until $(\text{current time} - \text{cycle start time}) \geq 0.05$ seconds, where cycle start time is the time recorded in Step 2.
2. Record the data logger’s current clock time as the cycle start time. The cycle start time is used to set the timeout the next time the program gets to Step 1.
3. For each barometer, execute a non-blocking read to retrieve the barometer measurement requested in Step 6 the previous cycle through the sampling loop. An empty or incomplete barometer I/O buffer is recorded as NaN to indicate bad data from the barometer.
4. Assemble the measurements obtained in Step 3 into an XML `<sample>` message. This involves associating a sample id number and a sample time-stamp to the pressure measurements.
5. Send the XML `<sample>` message to each connected client using a non-blocking write through a TCP socket. Possible connected clients include *dqtplot*, *dqpsdplot*, *dqtssave*, etc.
6. For each barometer, send a “P3” command (measurement request) to the barometer using a non-blocking write.

7. Get the data logger's current clock time (as a timeval struct for 10e-6 second resolution). This time value will become the time-stamp for the measurements to be requested in Step 6.
8. Increment the measurement id number.
9. Repeat from Step 1.

The loop in Table 1 achieves sample rate control and barometer synchronization as follows. Regarding sample rate control, all reads and writes (both to the barometers and to the socket connections) are non-blocking. Because of this, the entire sample loop (Steps 2-9 in Table 1) take less than 10e-4 seconds to complete. Hence the loop returns to Step 1 well before the 0.05 sample period expires. Regarding barometer time-stamping, if we assume there is a constant delay between sending a P3 command to a barometer and the time the measurement is collected and returned by the barometer (time delay = P3 command write time + sum of usb-to-serial latencies + sum of serial communication times + barometer processing time + measurement read time), then the recorded time-stamp, while it may not be exact in an absolute sense, is some nearly constant offset from being exact in an absolute sense. More important, because we want to treat the four barometers as an "array antenna" for trace velocity and infrasound angle-of-arrival estimation, it is not the absolute measurement time that matters, but rather it is the synchronization of the measurements that matters so that we can determine the relative time between wave front arrivals at the various barometers (as will be described in Section 5.3). Because the delay between sending a P3 command to a barometer and receiving back a pressure measurement response is the same for all barometers, all we need is for the P3 trigger commands in Step 7 to be issued to all barometers at the same time. While this is not possible in our setup, since each barometer is controlled through a separate VCP (virtual serial-communications port) on the USB-to-serial multiplexer, it is nearly achieved – the mean time to execute the for-loop of non-blocking P3 write commands in Step 7 is 9e-5 seconds.

5.2 Data Analysis and Visualization

The measurements collected from the array of barometers at an infrasound station by the *dqtsserver* daemon are saved by *dqtssave* as XML files. These files are shipped via LDM (<http://www.unidata.ucar.edu/software/ldm/>) from the data loggers to a data archive on the campus of the University of Massachusetts, Amherst, MA. As each new XML file is received, it is converted from XML to a tab delimited ASCII flat file that can be directly loaded into Matlab (registered trademark, Mathworks, Inc.). Matlab then performs the data processing leading to the operator displays. The basic processing done by the Matlab programs (colored orange in Fig. 14) are listed in Table 2.

Table 2. Matlab Infrasound Processing

1. Ingest the measurements from an infrasound station into Matlab.
2. Perform quality control to deal with NaNs (bad data), repeat values, etc.
3. Integrate the samples to improve the SNR. Note that in general we "oversample" (i.e., use a sample rate that is several times faster than the Nyquist rate needed for the

maximum frequency of interest) so that we can “integrate” (sum) multiple samples together. Similar to non-coherent integration in radar, this improves the SNR by constructive interference of the coherent infrasound signal and destructive interference of the incoherent barometer and background noise.

4. Generate a stacked plot of the last 30-seconds of time-series data from the four sensors in the array.
5. Generate a power-spectral-density (PSD) of the last 30-seconds of time-series data to give the operator a sense of whether or not there are coherent infrasound signals passing over the array.
6. Run an array-processing algorithm (frequency-wavenumber (F-K) analysis in our case) to obtain estimates for the trace velocity and back-azimuth, angle-of-arrival of any coherent signals passing over the array of sensors. The F-K analysis (to be described in Section 5.3), produces on a 30-second update cycle a correlation value, a trace velocity value, and an azimuth value and adds it to a plot that shows the evolution of these three quantities over the last 1/2-hour.
7. The correlation and back-azimuth information are displayed on top of the CASA merged composite reflectivity radar image so an operator can determine in real-time whether or not there are infrasound detections occurring inside the CASA radar test bed and if so correlate the infrasound detection to the radar data being observed at the same location.

Figs. 16 and 17 show the operator plots generated by the Matlab infrasound analysis programs.

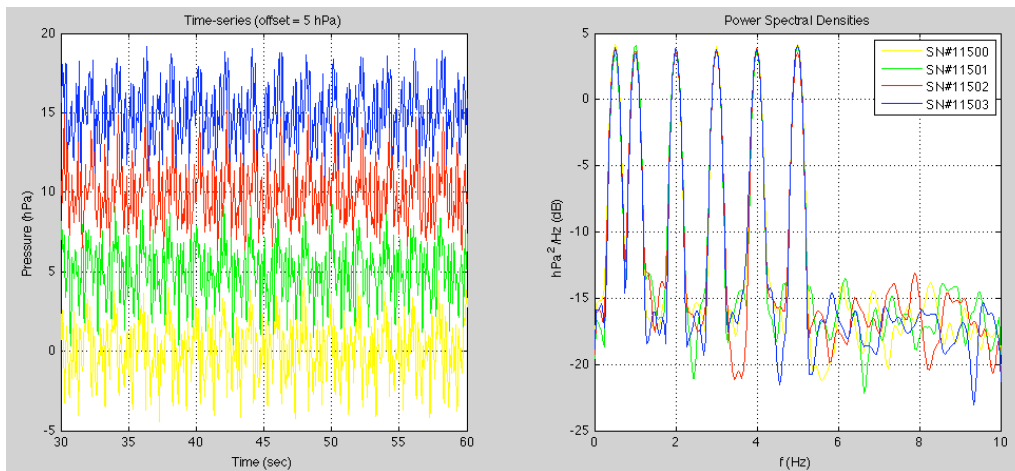


Fig. 16. Operator plot showing the last 30 seconds of data from the array of four barometers at an infrasound station (left) and the power-spectral-densities from the four barometers. In this case, there is (simulated) coherent infrasound at six different frequencies passing over the array.

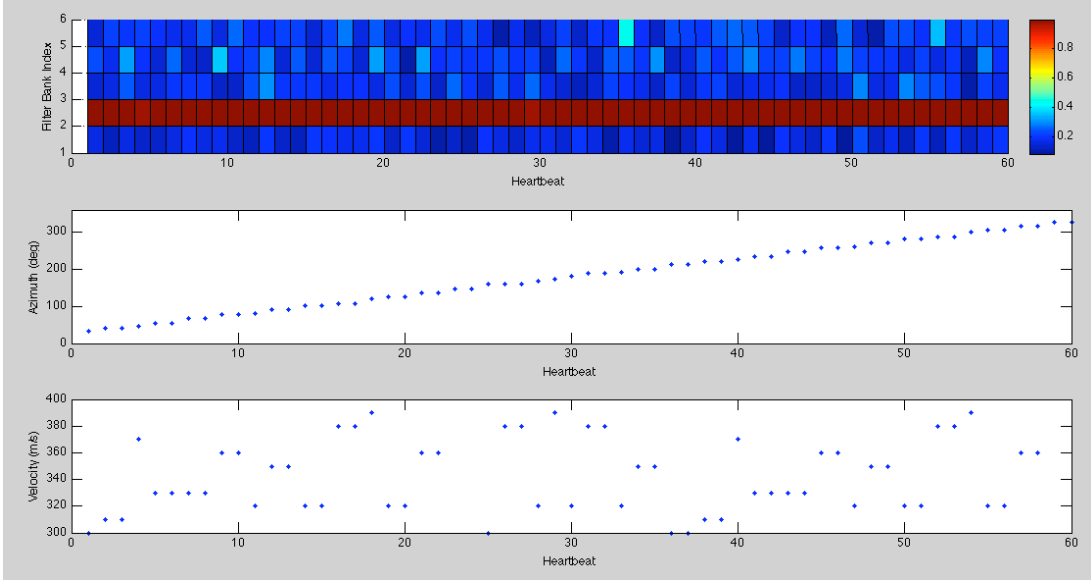


Fig. 17. Operator plot showing evolution of correlation (top), azimuth (middle), and trace velocity (bottom) over the last 1/2-hour of infrasound data. In these plots, the azimuth and trace velocity values are meaningful only when the correlation is high, and potentially irrelevant when the correlation is low. The azimuth and velocity curves were obtained by the F-K algorithm after filtering with band-pass filter number 2. This frequency-band contains an infrasound signal that is coherent across the array of sensors, as indicated by the high correlation value in the top plot.

5.3 F-K Analysis

The purpose of F-K analysis is to estimate the trace velocity and back-azimuth of an infrasound signal under the assumption that the infrasound source is sufficiently far from the infrasound array that its signal looks like a plane wave passing over the array (Rost and Thomas, 2002; Cansi and LePichon, 2009; Olson and Szuberla, 2009). A side benefit of F-K analysis is that it improves SNR through its process of signal phase alignment (which boosts the in-phase part of the signal while at the same time reducing the out-of-phase barometer noises). The basic idea of F-K analysis is that a signal arriving from azimuth direction θ at trace velocity v will arrive at each barometer at a slightly different time. If \mathbf{R} is the position matrix giving the location of each barometer relative to some reference location (e.g., the location of the GPS antenna that is connected to the data logger), then the arrival time difference at sensor i relative to the arrival time at the reference location is given by the matrix equation,

$$\boldsymbol{\tau} = \mathbf{R}\mathbf{u} \quad (1)$$

where \mathbf{u} is the so-called “slowness” vector,

$$\mathbf{u} = \begin{bmatrix} u_x \\ u_y \end{bmatrix} = \begin{bmatrix} \frac{1}{v} \cos(\theta) \\ \frac{1}{v} \sin(\theta) \end{bmatrix} \quad (2)$$

Thus, if we have the vector $\boldsymbol{\tau}$, then we can solve for the slowness vector \mathbf{u} , from which we get,

$$v = \frac{1}{\sqrt{u_x^2 + u_y^2}} \quad (3)$$

and,

$$\theta = \tan^{-1}\left(\frac{u_y}{u_x}\right) \quad (4)$$

In general, there are two ways to solve equation (1). One can estimate the pair-wise cross-correlations, do some peak finding to come up with a $\boldsymbol{\tau}$ vector, and then use least squares to solve for the slowness vector,

$$\mathbf{u} = (\mathbf{R}^T \mathbf{R})^{-1} \mathbf{R}^T \boldsymbol{\tau} \quad (5)$$

In this case, it is also necessary to check the consistency of the τ 's, since a valid set should sum to zero around any loop, e.g., in a three sensor array, one should have,

$$\mathbf{0} = \tau_{01} + \tau_{12} + \tau_{20} \quad (6)$$

where τ_{ij} is the time difference between the time of arrival of a wavefront at sensor i and sensor j .

As an alternative to the above "direct" approach, one can solve for \mathbf{u} "indirectly". The F-K algorithm is one such indirect approach (Rost and Thomas, 2002). The F-K algorithm does a grid search over a subspace of θ, v for the tuple that best time/phase-aligns the signals across the N barometers in the array. The criteria for assessing time/phase alignment is,

$$J(\theta, v) = \sum_{k=1}^L \left(\frac{1}{N} \sum_{i=1}^N x_i(k + \tau_{i0}(\theta, v)) \right)^2 \quad (7)$$

where k is the sample index, L is the data window size, i is the instrument (barometer) index, and the τ_{i0} are computed using $\boldsymbol{\tau} = \mathbf{R}\mathbf{u}(\theta, v)$ for the given θ, v pair under consideration. We also note that x_i is the recorded signal from barometer i , band-pass filtered to the frequency band of interest.

While generally the F-K algorithm is implemented in the frequency domain for speed and efficiency, it is worthwhile to write down the time-domain version of the algorithm for the intuition it gives. This appears in Table 3.

Table 3. Time-domain F-K algorithm.

1. Ingest $x_i(k)$ for each sensor, $i = 1, \dots, 4$.
2. Band pass filter the $x_i(k)$ to some frequency band that contains the signal of interest, e.g., (0.7, 1.3) Hz to bracket the 1-Hz tornado frequency band.
3. Set $\max J = -\infty$; $\text{THETA}^* = 0$; and $V^* = 0$;
4. For $\text{THETA} = [0, 360)$,
 - a. For $V = [300, 450]$,
 - i. Compute the time-shifts, $\text{TAU}_i = (1/V)(R_{x_i} \cos(\text{THETA}) + R_{y_i} \sin(\text{THETA}))$, where R_{x_i} is the x position of sensor i , and R_{y_i} is its y position;
 - ii. Set $J = 0$;
 - iii. For $k = 1$ to L
 1. Set $y(k) = 0$;
 2. For $i = 1$ to N ,
 - a. $y(k) = y(k) + x_i(k + \text{round}(\text{TAU}_i / f_s))$
 3. End
 4. $y(k) = y(k) / N$;
 5. $J = J + y(k) * y(k)$;
 - iv. End
 - v. If $J > \max J$,
 1. $\max J = J$; $\text{THETA}^* = \text{THETA}$; $V^* = V$;
 - vi. End
 - b. End
5. End
6. Report $\max J$, THETA^* , V^*

As seen in Table 1, the F-K algorithm is actually quite simple, performing a search over THETA and V for the set of time-shifts (computed in Step i) that maximize the array energy (computed in Step iii). The correctness of the algorithm is determined by whether or not maximizing the array energy, J , correctly finds the time shifts that give the relative arrival time of an infrasound wavefront at each sensor. For the case of a pure tone (sinusoid) it is clear that the set of time shifts that phase aligns the signals at the various barometers will maximize J , since phase alignment in the case of a pure tone maximizes J through constructive interference of the sinusoids from each barometer. Checking the phase alignment of the signals before and after running the F-K algorithm is actually a simple way to check the software for implementation errors. Although the consistency of the time-shifts is automatically satisfied by the F-K algorithm, an issue with the algorithm is that it will always return a solution, even in the case where there is no signal passing over the array that is coherent at all of the barometers. The usual way to check that the azimuth and trace velocity produced by the F-K algorithm are meaningful is to compute the mean pairwise correlations between the F-K time-shifted signals. If the mean correlation is high, then detection of an infrasound signal is announced and the azimuth and trace velocity provide meaningful information about the location of the infrasound emitter. To deal with

instabilities in the azimuth reported by the algorithm (e.g., due to sensor/wind noise, wide “beam-width” etc.), the F-K analysis is sometimes performed as an average over some number of overlapping data windows to “smooth” the azimuth and velocity results. See (Rost & Thomas, 2002) for details of array processing algorithms including the frequency domain version of F-K and its variants. We also point the reader to the MatSeis InfraTool, a Matlab implementation of the F-K algorithm downloadable from the website (<https://na22.nnsa.doe.gov/cgi-bin/prod/nemre/matseis.cgi>).

To illustrate the F-K algorithm, consider the array of four barometers laid out in an 80 x 80 meter square as in Fig. 9. Consider a 0.5 Hz signal arriving from $\theta = 35$, a 1 Hz signal arriving from $\theta = 66$, a 2 Hz signal arriving from $\theta = 290$, a 3 Hz signal arriving from $\theta = 190$, a 4 Hz signal arriving from $\theta = 50$, and a 5 Hz signal arriving from $\theta = 70$. Assume all signals are pure sine waves (no noise) and that the trace velocity is 340 m/s in each case. These signals and their PSDs are shown in Fig. 16. Fig. 21 shows the F-K analysis window.

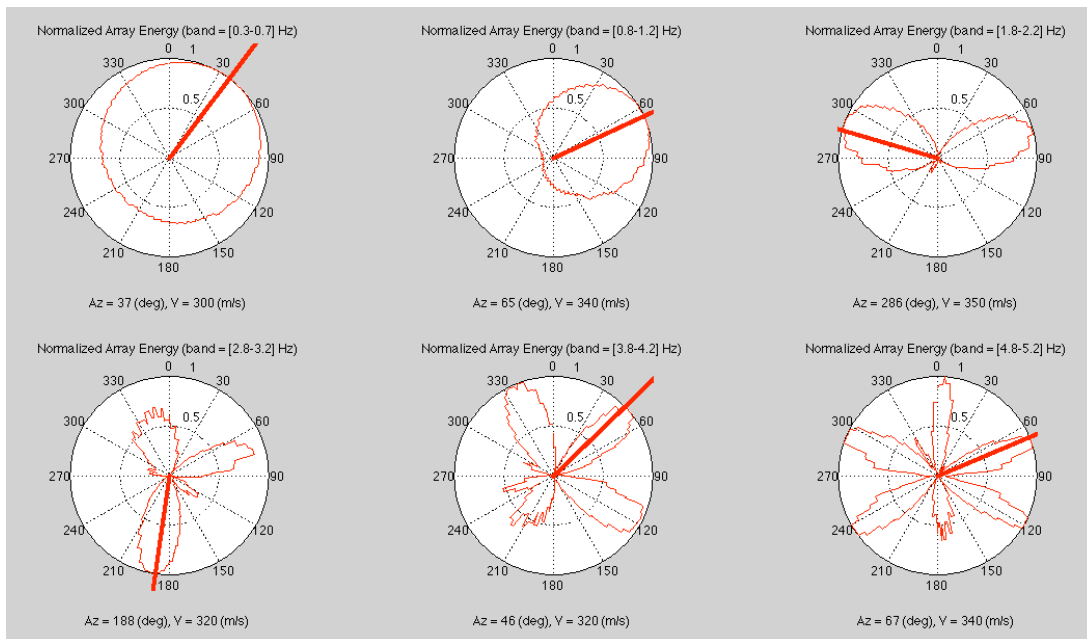


Fig. 21. F-K analysis window showing the back-azimuth angles associated with the maximum energy (the dark line) drawn over a plot of the maximum energies for each azimuth angle (normalized by the maximum energy over all θ and v). Each plot represents the results after filtering by a different band-pass filter.

One thing to notice in Fig. 21 are the normalized array energy curves. When the input signal is a pure sine wave, these curves approximate the beam pattern of the array. The narrowness of the beam gives an indication of the directivity of the array (the accuracy of its azimuth estimate). The number and magnitude of the side-lobes gives an indication of the possibility of azimuth errors due to the F-K algorithm settling on the wrong local maximum of the array energy. In Fig. 21, while the azimuth angles returned by the F-K algorithm were correct in each case, the side lobes being nearly as large as the main lobe in

the two “high” frequency plots in the lower right of Fig. 21 could easily have resulted in the F-K settling on an incorrect solution.

What is also evident in the normalized array energy curves in Fig. 21 is the dependency of the beam pattern on the frequency of the infrasound signal. For the lowest frequency of 0.5 Hz we have a very wide beam, meaning that the directivity is poor. As frequency is increased the beam first gets narrower, giving better directivity. However, as the frequency continues to increase, the beam pattern develops increasingly more and increasingly larger “grating” lobes. When the magnitude of these lobes reaches the size of the main lobe, direction ambiguities can result. Thus, we see an inverse relationship between frequency and size of the array aperture that gives good directivity; lower frequencies requiring larger aperture sizes, higher frequencies smaller ones. Generally, the inter-element spacing, d , between the barometers in an infrasound array should be chosen to be as large as possible, but no larger than $d = \lambda_{\min}/2$, where λ_{\min} is the wavelength ($\lambda = \text{speed of sound} / \text{signal frequency}$) of the highest frequency of interest. Any larger than this and there will be grating lobes, as in the lower right of Fig. 21. In this case, the frequency passing over the array is 5 Hz, corresponding to $d = 34$ m, which is much smaller than our 80 m aperture.

As a final comment, note that the array patterns in Fig. 21 were generated as a result of beam-forming with all four of the array elements. This is not necessary, and it may be possible to improve directivity if one does not use all of the array elements in the calculations. One element gives no direction information. Two elements give ambiguous direction (the pattern is symmetric about a line connecting the two elements). Three elements are the smallest set needed for unambiguous direction. Thus one can imagine beam-forming using different combinations of three array elements, and an array topology that allows one to choose a large aperture triple for the low-frequencies and a small aperture triple for the high-frequencies. While this cannot be done with a square topology, other topologies, such as a centered triangle (a four sensor array with a central sensor at the center of a triangle of three other sensors). This idea is similar in some respects to the PMCC algorithm, which is used in the 8 element CTBTO infrasound arrays (Cansi and LePichon, 2009). These arrays have a small triangular array surrounded by a large pentagonal array. This arrangement gives a large number of triples with a large number of different apertures. PMCC adds array elements to the beam estimation based on the value they add to the estimate. In this way the algorithm is able to choose the right size aperture for the signal of interest. Our final choice of array spacing and topology will be a compromise to try to get good directivity over the entire band of frequencies of interest, which we take as 0.5 Hz to 5 Hz for severe weather.

5 Summary

This paper described an experiment CASA will do in the spring of 2011 to integrate infrasound into its network of small weather radars in southwestern Oklahoma. The hardware and software developed for the experiment is undergoing final test at the University of Massachusetts, Amherst. Easement agreements are being negotiated with the landowners of the Oklahoma sites. Shipping will begin soon, with setup in mid-March. The

experiment itself will take place from April through June. The goal of the experiment is to understand the role of infrasound as an adjunct to other sensor data – radar, mesonet, human spotters, and so on – to improve weather hazard lead time, with particular focus on tornadoes. In relation to other work, this work revisits a study conducted several years ago by NOAA under its ISNet project but on a much more dense spacing – 30 km between sensors rather than 250 km between sensors. As the analysis in this paper showed, this more dense spacing should overcome the acoustic shadow coverage gap of infrasound that can result in an inability to detect a weather hazard infrasound sufficiently early to make it useful for operational early-warning decision making. Future papers will document the data collection experiences and present the detection results.

Acknowledgements

CASA is supported primarily by the Engineering Research Center program of the National Science Foundation (NSF) under NSF Cooperative Agreement EEC-0313747. Additional funding for this work is being provided by the Jerome M. Paros Fund for Measurement and Environmental Sciences Research and the NSF Research Experience for Undergraduates (REU) program.

References

- Bedard, A. J. (2005). Low Frequency Atmospheric Acoustic energy Associated with Vortices Produced by Thunderstorms. *Monthly Weather Review*, 241-263.
- Bedard, Jr. A. J., B. W. Bartram, B. Entwistle, J. Golden, S. Hodanish, R. M. Jones, R. T. Nishiyama, A. N. Keane, L. Mooney, M. Nicholls, E. J. Szoke, E. Thaler, D. C. Welsh, 2004b: *Overview of the ISNet Data Set and Conclusions and Recommendations from a March 2004 Workshop to Review ISNet Data*. Preprints of the American Meteorological Society, 22nd Conference on Severe Local Storms. Available on-line: http://ams.confex.com/ams/11aram22sls/techprogram/paper_81666.htm.
- Bedard Jr., A. J., B. W. Bartram, A. N. Keane, D. C. Welsh, R. T. Nishiyama, 2004a: *The Infrasound Network (ISNet): Background, Design Details and Display Capability as an 88D Adjunct Tornado Detection Tool*. Preprints of the American Meteorological Society, 22nd Conference on Severe Local Storms. Available on-line: http://ams.confex.com/ams/11aram22sls/techprogram/paper_81656.htm.
- Bedard Jr., A. and T.M. Georges, 2000: Atmospheric Infrasound. *Physics Today*, **53**, 32-37.
- Berchoff, D., 2010: *NWS Science and Technology Roadmap...Enabling the Future*. Presentation at the National MIC/HIC Workshop, Leesburg, VA, 20 May 2010. Available on-line at: http://www.weather.gov/ost/S&TRoadmap/docs/Berchoff_S&T%20Roadmap_MIC_HIC_20%20Apr%202010.pdf.
- Brewster, K.A., L. White, B. Johnson, and J. Brotzge, 2005: Selecting the sites for CASA NetRad, a collaborative radar network. Preprints, *Ninth Symp. on Integrated Observing and Assimilation Systems for the Atmosphere, Oceans, and Land Surface*, San Diego, CA, Amer. Meteor. Soc., P3.4 [Available online at: http://ams.confex.com/ams/Annual2005/techprogram/paper_86635.htm.]

- Brotzge, and coauthors, 2007: CASA IP1: Network operations and initial data. Preprints, 23rd Conf. on Interactive Information Processing Systems for Meteorology, Oceanography, and Hydrology, San Antonio, TX, Amer. Meteor. Soc. 8A.6 [Available online at: http://ams.confex.com/ams/87annual/techprogram/paper_120056.htm.]
- Brotzge, J., K. Hondl, B. Philips, L. Lemon, E. Bass, D. Rude, and D. Andra, Jr., 2010: Evaluation of Distributed Collaborative Adaptive Sensing for detection of low-level circulations and implications for severe weather warning operations. *Wea. Forecasting*, **25**, 173-189.
- Cansi, Y. and A. LePichon, 2009: Infrasound Event Detection using the Progressive Multi-Channel Correlation Algorithm. Book chapter in *Handbook of Signal Processing in Acoustics*, Springer, p. 1425-1435.
- Christie, D.R. and P. Campus, 2010: *The IMS Infrasound Network: Design and Establishment of Infrasound Stations*. In *Infrasound Monitoring for Atmospheric Studies*, Le Pichon, A., E. Blanc, and A. Hauchecome (Eds.), p. 29-75.
- Drob, D.P., 2003: *Global Morphology of Infrasound Propagation*. J. Geophys. Res. – Atmospheres, Vol. 108, No. D21, p. 4860.
- Kelleher, K., and D. Melendez, 2010: *NOAA Integrated Weather Radar Plan and 2025 Vision*. Presentation to the NOAA Science Advisory Board, 23 March 2010.
- McLaughlin D., D. Pepyne, V. Chandrasekar, B. Philips, J. Kurose, M. Zink, K. Droegemeier, S. Cruz-Pol, F. Junyent, J. Brotzge, D. Westbrook, N. Bharadwaj, Y. Wang, E. Lyons, K. Hondl, Y. Liu, E. Knapp, M. Xue, A. Hopf, K. Kloesel, A. DeFonzo, P. Kollias, K. Brewster, R. Contreras, B. Dolan, T. Djaferis, E. Insanic, S. Frasier, and F. Carr, 2009: Short-wavelength technology and the potential for distributed networks of small radar systems. *Bull. Amer. Meteor. Soc.*, **90**, 1797-1817.
- National Research Council, 1995: *Toward a New Weather Service: Assessment of NEXRAD Coverage and Associated Weather Services*. National Academies Press, 104 pp.
- National Research Council, 2002: *Weather Technology Beyond NEXRAD*. National Academies Press, 81 pp.
- National Research Council, 2004: *Where the Weather Meets the Road: A Research Agenda for Improving Road Weather Services*. National Academies Press, 174 pp.
- National Research Council, 2009: *Observing Weather and Climate from the Ground Up: A Nationwide Network of Networks*. National Academies Press, 250 pp.
- Olson, J.V. and C.A.L. Szuberla, 2005: *The Distribution of Wave Packet Sizes in Microbarom Wave Trains Observed in Alaska*. *The Journal of the Acoustical Society of America* **117**: 1032.
- Olson, J.V. and C.A.L. Szuberla, 2009: *Processing Infrasonic Array Data*. Book chapter in *Handbook of Signal Processing in Acoustics*, Springer, p. 1487-1496.
- Philips, B., V. Chandrasekar, J. Brotzge, M. Zink, H. Rodriguez, C. League, and W. Diaz, 2010: Performance of the CASA radar network during the May 13, 2009 Anadarko tornado. Preprints, *15th Symp. Meteor. Observ. Instrumentation*, Atlanta, GA, January 17-21, 2010.
- Philips, B. and coauthors, 2007: Integrating end-user needs into system design and operation: The Center for Collaborative Adaptive Sensing of the Atmosphere (CASA). Preprints, 16th Conf. on Applied Climatology, San Antonio, TX, Amer. Meteor. Soc. 3.14 [Available online at:

- http://ams.confex.com/ams/87Annual/techprogram/paper_119996.htm]
- Schaad, T., 2009: *Infrasound Signals Measured with Absolute Nano-Resolution Barometers*. Paroscientific, Doc. No. G8221 Rev. A. Available on-line: http://paroscientific.com/Environmental_Monitoring/g8221_nc.pdf.
- Schechter, D.A., M.E. Nicholls, J. Persing, A.J. Bedard Jr., and R.A. Pielke Sr., 2008: Infrasound emitted by tornado-like vortices: Basic theory and a numerical comparison to the acoustic radiations of a single-cell thunderstorm. *J. of Atmos. Sci.*, **65**, 685-713.
- Skowbo, E.A., D.C. Muh, and K.A. Fanto, 2009: *Infrasound Sensor System Detection of Atlas V Rocket Launch*. *Technology Review Journal*.
- Walker, K.T., and M.A.H. Hedlin, 2010: *A Review of Wind-Noise Reduction Methodologies*. In *Infrasound Monitoring for Atmospheric Studies*, Le Pichon, A., E. Blanc, and A. Hauchecome (Eds.), p. 141-181.
- Williams, E., 2010: Aviation Formulary. On-line at: <http://williams.best.vwh.net/avform.htm>.